



# Impact of membrane characteristics and chemical ageing on algal protein fouling behaviour of ultrafiltration membranes

Zainab Z. Mustafa<sup>a,b,c</sup>, Adrian T. Murdock<sup>c</sup>, Zongli Xie<sup>c</sup>, Geoffrey Johnston-Hall<sup>d</sup>, Rita K. Henderson<sup>a,b</sup>, Greg L. Leslie<sup>b</sup>, Pierre Le-Clech<sup>a,b,\*</sup>

<sup>a</sup> Algae and Organic Matter Laboratory (AOM Lab), School of Chemical Engineering, The University of New South Wales, Sydney, NSW 2052, Australia

<sup>b</sup> UNESCO Centre for Membrane Science and Technology, School of Chemical Engineering, The University of New South Wales, Sydney, NSW 2052, Australia

<sup>c</sup> CSIRO Manufacturing, Lindfield, NSW 2065, Australia

<sup>d</sup> DuPont™, South Windsor, NSW 2756, Australia

## ARTICLE INFO

Editor: V. Tarabara

### Keywords:

Ageing  
Chain scission  
Fouling  
Pore size  
Surface roughness

## ABSTRACT

Membrane characteristics can exacerbate the prevailing challenges associated with membrane fouling in industry. However, the combined impact of deliberate membrane modifications and the unavoidable effects of chemical ageing on fouling behaviour is still not well understood. In this study, three polyvinylidene fluoride (PVDF) ultrafiltration (UF) membranes with different pore size and surface roughness were selected and subject to chemical ageing with 5000 ppm sodium hypochlorite (NaOCl) at pH 10.5, selected to simulate accelerated ageing conditions. The impact of NaOCl on membrane characteristics was assessed for exposure times from  $1.2 \times 10^5$  to  $25.2 \times 10^5$  ppm-h using scanning electron microscopy (SEM), Fourier-transform infrared (FTIR) spectroscopy, contact angle, and clean water resistance analysis. The fouling behaviour of each pristine and aged membrane was compared using 10 mg C.L<sup>-1</sup> dissolved organic carbon algal protein feed containing 18 % biopolymeric compounds. The membrane with intermediate pore size presented lower overall filtration resistance compared to the membrane with smaller pores that developed rapid foulant cake layers. It also displayed less susceptibility to fouling via pore blocking mechanisms compared to membranes with larger pores where greater surface area available in pore walls leads to higher foulant adhesion.

## 1. Introduction

Changing membrane characteristics such as pore size, surface roughness, porosity, and hydrophilicity can significantly impact membrane fouling behaviour [26,23,9]. The selection of suitable membrane characteristics is thus essential to efficiently manage fouling in industry and prevent early membrane failure [48,28]. Membrane characteristics can be modified either deliberately through controlled modifications such as surface modifications and polymer blending during manufacturing or by unavoidable changes due to membrane ageing [56].

Membrane modifications via tuning of fabrication conditions such as the composition of casting polymer solutions and the solvent to non-solvent ratio [52,6] is one of the simpler methods of inducing changes in morphology such as pore size, porosity, and roughness [58]. These adjustments in membrane fabrication can thus be used to fine-tune

membrane properties to provide selected advantages such as low filtration resistance or low chemical cleaning demand [28,34], hence offering high value for membrane manufacturers and plant operators alike.

Sodium hypochlorite (NaOCl) is commonly used as a cleaning agent to remove adsorbed foulants from microfiltration (MF) and ultrafiltration (UF) membranes in water and wastewater treatment applications. Exposure to NaOCl in industry is recognised to induce membrane ageing, leading to changes in physical and chemical properties during operation [39,37,51]. These changes can result in higher chemical cleaning demand, gradual accumulation of irrecoverable fouling, and eventually, membrane integrity loss [45,42]. Despite the inevitable impact of chemical ageing on membranes, the phenomenon is still poorly understood due to limited research in the membrane ageing field [59,3].

Polyvinylidene fluoride (PVDF) membranes are well regarded in

\* Corresponding author at: Algae and Organic Matter Laboratory (AOM Lab), School of Chemical Engineering, The University of New South Wales, Sydney, NSW 2052, Australia.

E-mail address: [p.le-clech@unsw.edu.au](mailto:p.le-clech@unsw.edu.au) (P. Le-Clech).

<https://doi.org/10.1016/j.seppur.2024.128481>

Received 18 February 2024; Received in revised form 14 June 2024; Accepted 16 June 2024

Available online 24 June 2024

1383-5866/© 2024 The Authors. Published by Elsevier B.V. This is an open access article under the CC BY license (<http://creativecommons.org/licenses/by/4.0/>).

industry for their high resistance to chemical degradation [50,33,57]. Previous studies mainly aimed to simulate and understand the chemical and physical degradation of PVDF membranes with NaOCl exposure in industry [11,47]. Various ageing mechanisms have been proposed for physical changes in membrane characteristics with chemical age. Studies have reported an increase in membrane pore size along with an increase in membrane surface roughness with NaOCl exposure [29,53,41], attributed to the detachment of hydrophilic additives from the PVDF polymer framework and potential polymer chain scission [5,56]. Studies also report PVDF degradation via polymer cross-linking [41], and dehydrofluorination [16,14]. However, discrepancies on the impact of NaOCl exposure on PVDF membrane characteristics exist due to variation in membrane preparation protocols and the performance indicators used [26,45,15].

Limited research has been conducted on the resilience of different hydrophilic PVDF membranes to chemical exposure and subsequent fouling behaviour [53]). Given the large range of commercially available PVDF membranes, and the expected discrepancies between their performance and fouling behaviour, it is critical to further study this important topic, so to ultimately provide operators with advice and recommendations on membrane replacement. Previous studies have compared PVDF with other membrane materials such as polysulfone [12,57] and polyethersulfone [30]. Some studies have compared PVDF membranes formed via the two common PVDF fabrication techniques non-solvent induced phase separation (NIPS) and thermally induced phase separation (TIPS) [53,56]. However, no previous work has compared the impact of NaOCl ageing across different hydrophilic, asymmetric PVDF membranes, all fabricated via the NIPS technique, to understand the impact of changes in membrane characteristics via fine-tuning fabrication conditions on PVDF membrane fouling performance. Moreover, most previous studies do not apply initial membrane stabilisation protocols that may result in discrepancies across literature. In this study, three PVDF UF membranes, all fabricated via the NIPS technique presenting different pore size and surface roughness, were

stabilised via an initial rinsing procedure and assessed for their relative fouling behaviour with extended 5000 ppm NaOCl exposure time at pH 10.5.

The aim of this study was thus to (a) assess the impact of pore size and surface roughness of three PVDF membranes on fouling behaviour, (b) identify the impact of 5000 ppm NaOCl exposure at pH 10.5 on the physical and chemical surface characteristics of the three PVDF membranes, and (c) assess the subsequent impact of changing surface characteristics with NaOCl exposure on the fouling behaviour of each PVDF membrane.

## 2. Methods and materials

### 2.1. Membranes and ageing protocol

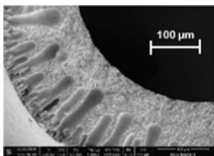
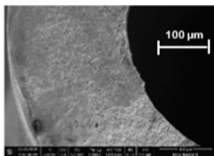
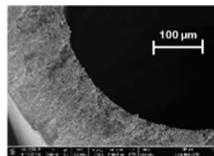
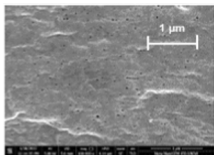
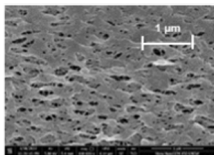
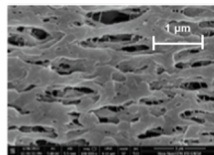
#### 2.1.1. Membranes

Three types of PVDF UF hollow fibre membranes, all fabricated via and termed 'M1', 'M2' and 'M3', were used for comparison in this study. All membranes were hydrophilic and featured a negative zeta potential (Table 1). Nominal pore size, determined by molecular weight cut off, ranged from 20 to 40 nm for M1 and M2 to approximately 80 nm for M3 (Table 1). Surface area and pore volume were measured using methods described in Section S3. Details on the method of membrane manufacture could not be disclosed due to confidentiality. All new membrane modules were activated with 20 % ethanol, then rinsed for 16 h at 100 L·m<sup>-2</sup>·h<sup>-1</sup> with deionised water and stored soaked in deionised water before use.

#### 2.1.2. Membrane characterisation

SEM (Nova NanoSEM 450) was used to visually examine changes in surface pore size, structure, and resulting roughness. Prior to imaging, samples were sputter coated with a 5 nm chromium sublayer followed by 5 nm platinum surface coat. Imaging was conducted at a beam voltage of 15 kV. For each sample, 3 images were collected from

**Table 1**  
Summary of membrane characteristics for three PVDF UF membranes.

UF PVDF Membrane	Membrane 1 (M1)	Membrane 2 (M2)	Membrane 3 (M3)
External diameter (mm)	0.85	0.97	0.85
Wall thickness (mm)	0.16	0.28	0.16
Membrane cross-section <sup>a</sup>			
Membrane surface <sup>a</sup>			
Permeability (L·m <sup>-2</sup> ·h <sup>-1</sup> ·bar <sup>-1</sup> )	967 ± 75	614 ± 70	1,395 ± 70
Zeta potential (mV) at pH 6–8	−17 ± 4	−25 ± 5	−25 ± 5
Contact angle <sup>b</sup> (°)	34 ± 6	27 ± 7	43 ± 3
Max pore size <sup>c</sup> (nm)	20–40	20–40*	~ 80
Pore volume <sup>d</sup> (cm <sup>3</sup> ·g <sup>-1</sup> )	0.05	0.09	0.22
Surface area <sup>d</sup> (m <sup>2</sup> ·g <sup>-1</sup> )	35	61	150

<sup>a</sup>Membrane cross-section and surface imaged using scanning electron microscope. Cross-sectional images taken at 1000x magnification. Surface images taken at 100,000 × magnification.

<sup>b</sup>Relative contact angle of hollow-fibre membranes measured using a tensiometer in the meniscus measurement mode, see Section 2.1.2 for details.

<sup>c</sup>Maximum pore size defined as the spherical particle size that has a 90% rejection by the membrane (Section S2).

<sup>d</sup>Relative pore volume and surface area estimated by Brunauer-Emmett-Teller (BET) adsorption curve. See Section S3 for details on calculation method.

\*See Section S1 for details on the MWCO analysis method and rationale for similar max pore size across M1 and M2 membranes.

different locations on the sample fibre, and all fibre samples were analysed with duplicates. Fibres were assessed for defects and irregularities both visually and using the SEM before images were captured.

Contact angle for the hollow fibre membranes was determined using a procedure similar to that applied previously [49]. An automated optical tensiometer (Theta ATA Scientific) was used in the single-fibre meniscus mode. Rinsed membranes were kept fully submerged in deionised water prior to testing. A steel rod reinforcement was used to ensure the hollow fibres remained vertical during the contact angle measurement. The wet membranes fibres were lowered into a pool of deionised water and then held in place for 3 s before recording the membrane-water interface contact angle. Recordings were taken for 3 s with 15 data points collected per second. This procedure was repeated at least 5 times along the length of the fibre sample and the results were averaged. Error was calculated from the standard deviation of contact angles across the 10 measurements for each data point.

FTIR spectroscopy (Spotlight 400, Perkin Elmer) was conducted using the attenuated total reflectance method (ATR) recorded over the range of 4000  $\text{cm}^{-1}$  to 650  $\text{cm}^{-1}$  (16 scans at 4  $\text{cm}^{-1}$ ) with all samples analysed with duplicate measurements. For SEM and FTIR analysis, all samples were lyophilised prior to testing. Ageing NaOCl (12.5 %, ChemSupply Australia) was used as the chemical ageing solution, diluted to a concentration of 0.5 % in deionised water. Static ageing tests were conducted by immersing membranes in excess NaOCl solution and storing in the absence of light at room temperature. Due to the gradual loss of free-chlorine in NaOCl, the concentration was monitored daily using a calibrated colorimeter free-chlorine measurement (Hach, Australia), and the solution was changed if the concentration dropped below 10 % of the original value. During industrial operation, cumulative exposure of NaOCl can range from  $5 \times 10^5$  ppm-h to  $2 \times 10^6$  ppm-h [3] for a PVDF membrane lifetime of approximately 5–10 years [45,3]. [57]. To simulate this, membranes M1, M2, and M3 were soaked continuously for 1, 3, 7, 14, and 21 days in 0.5 % NaOCl solution (5000  $\text{mg}\cdot\text{L}^{-1}$  free chlorine, pH 10.5) corresponding to NaOCl exposures of 1.2, 3.6, 8.4, 16.8, and  $25.2 \times 10^5$  ppm-h (Table 2). The NaOCl solution concentration (5000 ppm) and pH (up to 10.5), were chosen to accelerate the aging process [57], however, we note that these are higher than typical operating conditions used or recommended by membrane manufacturers [3].

## 2.2. Fouling analysis

### 2.2.1. Feed

Algal protein (food grade, PlantFusion) feed solution was prepared by dissolving in deionised water and centrifuging at 5500 rpm and 21 °C for 35 min. The supernatant was decanted, vacuum-filtered through a pre-rinsed 0.45  $\mu\text{m}$  polyester filter (Whatman, Australia) and diluted to a final dissolved organic carbon (DOC) concentration of 10  $\text{mg}\cdot\text{C}\cdot\text{L}^{-1}$  and maintained at neutral pH. The algal protein feed solution DOC consisted of 18 % biopolymer compounds (BP) (molecular size > 10,000 Da), 27 % intermediate molecular weight compounds (IMWC) (molecular size 300 – 10,000 Da), 39 % low molecular weight neutrals (LMWN) (molecular size < 350 Da), and 16 % hydrophobic organic compounds (HOC), as characterised by liquid chromatography organic carbon detection (LC-OCD). Unfortunately, a direct comparison between algal protein size and membrane pore size was not possible because of different size parameters used to define pore size and protein size.

**Table 2**

Actual concentration and contact time for NaOCl exposure in accelerated chemical ageing tests.

Contact time (days) with 5000 ppm NaOCl	1	3	7	14	21
Total exposure ( $\times 10^5$ ppm-h)	1.2	3.6	8.4	16.8	25.2

### 2.2.2. Filtration and fouling assessment

Filtration of algal protein solution was conducted using a bench-scale submerged membrane filtration system operated in outside-in mode (shell feed). Previous studies [8,10] reported the need for constant flux experiments for membrane fouling evaluation instead of constant pressure due to the impact of volume and flux bias in the latter operation mode. Thus, a constant flux of  $75\text{ L}\cdot\text{m}^{-2}\cdot\text{h}^{-1}$  was applied for all filtration experiments and fouling was monitored through transmembrane pressure (TMP) measurement. A permeate backwash was conducted every 2 h for 2 min at  $100\text{ L}\cdot\text{m}^{-2}\cdot\text{h}^{-1}$  that completed 1 ‘cycle’. After each backwash, permeate was returned to the feed beaker and the next cycle was started. Each fouling experiment was conducted for 6 cycles or until a TMP of 40 kPa was reached. The membranes were relaxed overnight after the 3rd cycle. During filtration, flux and TMP were logged automatically at 5 min intervals, and the feed was stirred with a magnetic stirrer at 50 rpm. All experiments were conducted at room temperature of 25 °C and resistance calculations were normalised at 25 °C.

Filtration models to evaluate potential pore blocking and cake filtration mechanisms from TMP profiles were developed according to the procedure detailed in a previous study [35]. Filtration models included complete blocking, standard blocking, intermediate blocking, and cake filtration. The error in the linearity correlation coefficient ( $R^2$ ) was calculated using duplicate assessment of the unaged M3 membrane across both cycle 1 and cycle 6 with all four filtration models.

Fouling rate was defined as the change in TMP over time while resistance was linearly proportional to TMP at constant flux. Details on the calculation of fouling rate, resistance, and rejection can be found in a previous study [35]. Experimental variations in fouling rate, resistance and rejection were determined from triplicate fouling analysis of the unaged M3 membrane. The unaged M3 membrane was used to determine error across all membrane types because error in these experimental variations is assumed to be independent of membrane type.

Clean water resistance measurements were conducted at  $100\text{ L}\cdot\text{m}^{-2}\cdot\text{h}^{-1}$  using deionised water, calculated after 1.5 min of continuous filtration to ensure membrane resistance stabilisation. Where change in resistance was below 0.3 kPa, the error was calculated as the standard deviation of TMP over 3 min filtration with data logging at 30 s intervals. For change in resistance above 0.3 kPa, standard deviation error was collected from triplicate clean water resistance measurements.

Rejection of organic size fractions was determined by LC-OCD characterisation of the feed and filtrate as per the procedure for LC-OCD analysis applied previously [36]. Feed was sampled before the filtration commenced, while the filtrate was sampled after all filtration cycles were completed. Analytical variation in LC-OCD characterisation was assessed using triplicate samples for the unaged M3 membrane.

### 2.2.3. Backwash and chemical cleaning

Reversibility after backwash was calculated as per Equation (4.1) [43], where  $TMP_{ini}^n$  was the TMP at the beginning of cycle  $n$ ,  $TMP_{end}^n$  was the TMP at the end of cycle  $n$ , and  $TMP_{ini}^{n+1}$  was the TMP at the beginning of the next cycle  $n + 1$ . The reversibility after backwash for each cycle was then averaged to determine the average reversibility after backwash. Reversibility after overnight relaxation (cycle 3) was omitted to indicate backwash efficiency only. Error in the reversibility after backwash was calculated as the standard deviation in reversibility over the filtration cycles for each fouling experiment. The term ‘TMP recovery’ was used interchangeably with ‘reversibility after backwash’.

$$\text{Reversibility after backwash}(\%) = \frac{TMP_{end}^n - TMP_{ini}^{n+1}}{TMP_{end}^n - TMP_{ini}^n} \times 100 \quad (4.1)$$

Chemical cleaning was carried out after the final filtration cycle was completed. The membrane was manually rinsed with deionised water to remove loosely bound proteins, backwashed with filtrate for 3 min at  $100\text{ L}\cdot\text{m}^{-2}\cdot\text{h}^{-1}$  and then cleaned by soaking in NaOH 0.01 % for 2 h with stirring at 50 rpm. NaOH was specifically used for the cleaning process

so that the resulting cleaning solution could undergo organic assessment via LC-OCD analysis. This is because free chlorine can disrupt the elution of organic material through the size exclusion column. NaOCl was the accelerated ageing agent used in this study. NaOH exposure was considered negligible to that of NaOCl and was kept constant in all results. A comparison of membrane ageing mechanisms with exposure to NaOCl and NaOH has been explored in another study [53]. After cleaning, a clean water resistance test using deionised water was conducted to determine the resistance of the chemically irreversible fouling layer (CIFR) after subtracting the known resistance of the membrane. Error in the CIFR was calculated as the sum of the standard deviation of clean water membrane resistance measurements before and after fouling.

3. Results and discussion

3.1. Impact of membrane characteristics on fouling behaviour

3.1.1. Fouling rate

The TMP profiles for the three PVDF membranes M1, M2, and M3 (Fig. 1) were used to compare the fouling behaviour of the membranes with algal protein feed solution. M2 was found to present the lowest TMP rise for all 6 filtration cycles and M1 generally displayed the highest TMP rise per cycle, however, the performance of M3 was observed to change significantly from cycles 1–3 to cycles 4–6. For cycles 1–3, the TMP rise per cycle was in the order M1 (~9 kPa/cycle) > M2 (~3 kPa/cycle) > M3 (~2 kPa/cycle), however, for cycles 4–6, while the TMP rise per cycle for M1 and M2 was similar to the respective TMP rise per cycle in cycles 1–3 (~13 kPa/cycle for M1 and ~5 kPa/cycle for M2), M3 displayed a rapid change in fouling behaviour in cycles 4–6 (~10 kPa/cycle). In the initial 3 cycles, the higher TMP rise for M1 and M2 relative to M3 was likely due to the smaller pore size of M1 and M2 (Table 1) that is known to result in higher short-term fouling resistance [27,7]. Furthermore, M2 presented lower overall magnitude of resistance compared to M1. This is because M2 has lower TMP increase compared to M1 and due to that, the overall magnitude of resistance accumulated over the filtration cycles is also lower, since TMP and resistance have a linear correlation. This could be a result of a lower relative pore size in M1 compared to M2 as seen on the SEM images (Table 1) that could lead to higher overall filtration resistance in M1 due to the more rapid development of foulant cake layers over smaller pores [24]. Moreover, the lower magnitude of filtration resistance accumulated in M2 may also be a result of the higher visible surface roughness of M2 (Table 1) that had the potential to temporarily shield functional pores from approaching foulants, thus reducing the fouling accumulation on the membrane surface [17]. For M3, with extended cycles, the larger pores of the membrane compared to M2 were more susceptible to the consequences of pore blocking [31,44], including the potential to

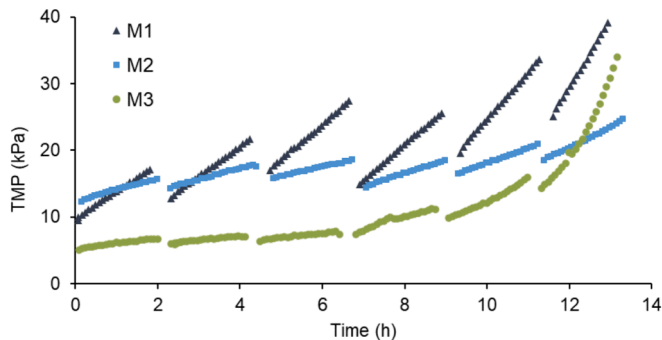


Fig. 1. TMP profile for membranes M1, M2, and M3. Filtration cycles conducted at 75 L·m<sup>-2</sup>·h<sup>-1</sup> with a backwash every 2 h for 2 min at 100 L·m<sup>-2</sup>·h<sup>-1</sup>. Filtration was conducted for 6 cycles or until 40 kPa was reached, with an overnight relaxation after the 3rd cycle.

increase the fouling resistance at an exponential rate [24], as it was observed (Fig. 1). Thus, while the membranes with smaller pores presented higher initial fouling resistance, larger pores were observed to accumulate fouling and lead to more severe fouling during extended cycles. Therefore, considering that an increase in pore size could provide lower filtration resistance but also a higher susceptibility to pore blocking, an intermediate pore size would present ideal results and could explain the optimal results observed for M2 (Table 4).

The TMP profiles (Fig. 1) were further applied to examine the relative reversibility of each membrane by relaxation (conducted after cycle 3) and backwash with respect to their physical surface properties. Relaxation was effective for TMP recovery in both M1 and M2 but not M3. The average backwash reversibility of the membranes followed the order M1 > M3 > M2. For both M1 and M2, the TMP at the start of cycle 4 was lower than the TMP at the start of cycle 3, whereas for M3, the TMP at the start of cycle 4 was higher than the TMP at the start of cycle 3. This implied that the overnight relaxation between cycles 3 and 4 led to the recovery of over 100 % of the TMP accrued in the previous cycle for M1 and M2, however, for M3 there was minimal TMP recovery after overnight relaxation. This indicated that the membranes with smaller pore sizes had fouling layers that could be easily detached, underscoring that the effectiveness of membrane relaxation to mitigate fouling development can vary depending on membrane characteristics. In contrast, larger pore size in M3 likely induced greater fouling adsorption on pore walls and pore blocking, due to the ability for foulants to enter larger pores, that subsequently reduced fouling reversibility [31,23]. However, the average TMP recovery after backwash for all other cycles excluding overnight relaxation was lowest for M2 (~35 %), followed by M3 (45 %) and M1 (~55 %) (Fig. 1). Lower backwash efficiency in the case of M2 was likely due to the greater surface roughness of this membranes that provide greater surface area for foulant attachment [28,18], thus reducing the efficiency of physical cleaning. Therefore, smaller pore size and lower surface roughness properties were found to provide higher physical fouling reversibility (Table 4). However, for membranes with larger pore size and rougher surfaces, greater backwash frequency may be required to control fouling development with extended cycles. It is important to note that only a qualitative assessment of surface roughness has been applied via SEM analysis in this study. Detailed characterisation is suggested in future work to provide a more quantitative assessment of surface roughness across the membranes.

3.1.2. Filtration models

Potential fouling mechanisms leading to distinct fouling behaviours across the membranes were further investigated using linear correlations with four filtration models (Table 3). In cycle 1, M2 presented higher correlations with all filtration models compared to M3, whereas after 6 cycles, both M1 and M2 were found to display a high correlation ( $R^2 > 0.99$ ) with all filtration models. Thus, across the 6 cycles, while the

Table 3  
Linearity correlation coefficient ( $R^2$ ) of four filtration models with the fouling profile for membranes M1, M2, and M3 in the first filtration cycle and last filtration cycle. Error in the  $R^2$  value across identical fouling experiments was up to 0.01.  $R^2$  values of '1.00' represent  $0.999 \geq R^2 \geq 0.995$ . Equations corresponding to each model can be found in previous work [35].

Linearity ( $R^2$ )		M1	M2	M3
Filtration Cycle 1	Complete blocking	0.97	0.97	0.95
	Standard blocking	0.98	0.98	0.96
	Intermediate blocking	0.99	0.98	0.96
	Cake filtration	1.00	0.99	0.97
Filtration Cycle 6	Complete blocking	0.97	1.00	1.00
	Standard blocking	0.99	1.00	1.00
	Intermediate blocking	0.99	1.00	1.00
	Cake filtration	0.99	1.00	1.00



correlations with pore blocking and cake filtration for M2 were similar for most filtration models, the correlations for M3 were found to differ more notably. In cycle 1, M3 displayed a higher correlation with cake filtration compared to complete blocking, however, in cycle 6, the same membrane displayed a notably higher correlation with all models. This indicated that the increased effect of pore blocking was one of the primary mechanisms driving the higher fouling observed in M3 with extended filtration cycles (Fig. 1). The model thus reaffirmed the potential adsorption of foulants on pore walls for larger pores in M3, as per the mechanisms of the standard blocking filtration model, as was hypothesized in Section 3.1.1. Though M2 also presented high correlations with pore blocking models, the larger pore size of M3 likely aggravated the pore blocking mechanism over the fouling cycles [32,22] and subsequently produced a more severe and incompressible fouling layer [25,4]. It is important to note that, considering M2 displayed a high correlation with all pore blocking models after 6 cycles, a fouling behaviour like M3 could be anticipated for M2 with extended filtration [1,25] especially due to the high surface roughness of M2 [23]. Moreover, the lower fouling reversibility of M2 (Section above) and varying cross-sectional structure of the membranes where M2 presented the highest wall thickness (Table 1) could indicate the impact of a depth filtration effect caused by the morphology of the membrane selective and support layers on the fouling performance particularly in M2 {Kumar, 2015 #899} (Section S1). Therefore, while the fouling behaviour of M3 was likely exacerbated by pore blocking in larger pores, high correlations of pore blocking also found with the M2 membrane and the potential for increased fouling complexity due to internal membrane morphology indicated potential fouling challenges with extended filtration for M2 (Table 4).

M1 was found to present higher correlations with intermediate pore blocking and cake filtration fouling mechanisms compared to complete blocking (Table 3). In contrast to M2 and M3, the correlations were not found to change significantly from cycle 1 to cycle 6. The preferential role of intermediate pore blocking and cake filtration over complete blocking indicated the development of a porous cake layer for M1, likely due to smaller membrane pores that increased likelihood of foulant attachment to the membrane surface or other foulants in preference to pores [24]. This could be contrasted to the previously discussed incompressible cake layer development in the case of M3 due to larger pore size. Furthermore, the lack of significant change in fouling mechanisms or degree of correlation to filtration models with consecutive cycles suggested that the fouling performance was relatively stable for M1. This stability could be attributed to the smoother surface for this membrane that entrapped less foulants and thus provided less opportunity for change in fouling mechanisms or fouling aggravation due to the interaction of foulants with pre-deposited fouling layers [21,49].

**Table 4**

Summary of the impact of membrane characteristics for M1, M2 and M3 on algal protein fouling behaviour and proposed mechanisms to explain behaviour.

	Distinctive Characteristic	Fouling behaviour	Proposed Mechanisms
M1	Small pores	High filtration resistance.	Small pores induce higher immediate resistance.
	Smooth surface	High backwash reversibility.	Smooth surface provided less opportunity for foulant adhesion.
M2	Rough surface	Low backwash reversibility.	Rougher surfaces can entrap foulants.
	Small pores (larger than M1)*	Medium filtration resistance.	Larger pores provide lower overall filtration resistance than smaller pores but more potential for fouling by pore blocking.
M3	Large pores	Low filtration resistance. Exponential increase in fouling rate	

\* As per the results of SEM and BET analysis, see Section S1 for details.

However, the high correlation of all models could imply that the fouling mechanisms occurred simultaneously, as has been reported for both single foulant and complex feedwater systems on UF membranes [19,20]. Various models used to evaluate the combined filtration mechanisms have been proposed [20] including a simplified technique to identify dominant fouling mechanisms through piecewise multiple linear regression modelling [55]. These advanced filtration models are thus recommended for analysis alongside the typical models in future work.

### 3.2. Impact of hypochlorite ageing on membrane characteristics

#### 3.2.1. SEM

The impact of 5000 ppm NaOCl exposure on the surface morphology of the three membrane was observed visually for no exposure,  $8.4 \times 10^5$  ppm·h, and  $25.2 \times 10^5$  ppm·h exposure (Fig. 2). Changes that could be observed visually were subtle for M1, and more apparent for M2 and M3, where M2 and M3 were found to display contrasting changes in surface roughness. Though some pore enlargement may be observed with the highest exposure for M1, the changes were subtle and inconclusive through SEM observation. It should be noted that imaging variations in pore morphology and roughness in M1 may have required additional image definition that was otherwise limited by the 10 nm conductive surface coating used for analysis. In M2, a higher surface porosity could be identified with increased exposure, where smaller pores in the framework were found to increase in size and the overall surface became visibly rougher. This increase in pore size and roughness has been proposed to be a result of the dislodgement of additives from the membrane [56,53,41] and potential chain scission in the PVDF framework [40]. For M3, surface deformation was observed and a gradual ‘smoothing’ of the surface with some visible reduction in smaller pores. Surface deformation resulting in the reduction in smaller pores and decreased surface roughness has previously been attributed to degradation via cross-linking in the PVDF macromolecular chains after additive loss [13]. It is important to note that the cross-linking PVDF degradation mechanism proceeds at a much slower rate compared to polymer chain scission in the presence of NaOCl [41], and thus further analysis is required to confirm that cross-linking takes place in the M3 membrane. Thus, while changes were inconclusive for M1, M2 displayed an increase in pore size and surface roughness, and surface deformation in M3 led to a potential reduction in small pores and decreased overall surface roughness (Table 5).

#### 3.2.2. FTIR

FTIR spectra depicting the impact of NaOCl exposure was presented for M3 (Fig. 3) while the spectra for M1 and M2 can be found in Section S4. For all membranes, a notable decrease in peak intensity with increasing chemical exposure was observed around  $1670 \text{ cm}^{-1}$ , while a reduction in peak intensity around the PVDF fingerprint region was observed for M2 and M3 but not M1. The reduction in intensity at  $1670 \text{ cm}^{-1}$  is generally attributed to carbonyl groups from hydrophilic polyamide additives such as polyvinylpyrrolidone (PVP) used in PVDF membrane synthesis, thus indicating the reduction of hydrophilic additives from all membranes when exposed to NaOCl [15,38] (Table 5). Furthermore, for M2 and M3, peak reductions were found in the PVDF fingerprint region, particularly  $1070 \text{ cm}^{-1}$  [13], signifying potential chemical attack on the PVDF macromolecular structure through potential chain scission or cross-linking [15,53]. The M1 membrane did not display a significant reduction in peak intensity in the PVDF fingerprint region, potentially indicating that the PVDF framework in M1 was less impacted by chemical exposure compared to M2 and M3. This corresponded with the SEM images that displayed less surface deformation in the M1 membrane compared to M1 and M2 (Fig. 2). It is important to note that despite additive loss with NaOCl exposure observed for all membranes here, the additives remained after the highest exposure. This indicated that while some reduction in

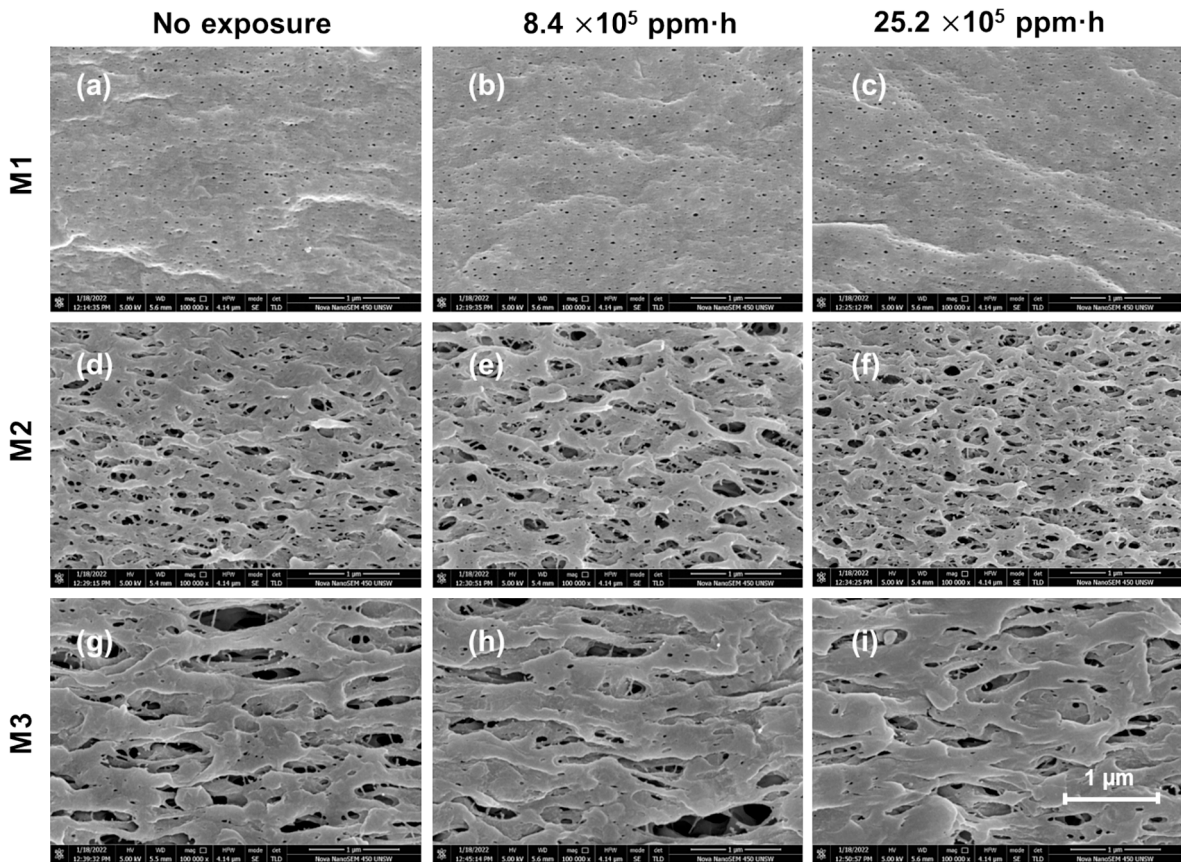


Fig. 2. SEM imaging of M1 (a, b, c), M2 (d, e, f), and M3 (g, h, i) for no NaOCl exposure (a, d, g),  $8.4 \times 10^5$  ppm·h (b, e, h), and  $25.2 \times 10^5$  ppm·h (e, f, i). Approximate image width of 4 μm at 100,000 × magnification.

Table 5				
Summary of the impact of increasing NaOCl exposure time at pH 10.5 on membrane characteristics as observed by SEM, FTIR, contact angle, and clean water resistance.				
	SEM	FTIR	Contact angle	Clean water resistance
<i>Increasing exposure till <math>8.4 \times 10^5</math> ppm·h (inclusive)</i>				
M1	Inconclusive	Reduction in additives	No significant change	Fluctuating decrease/inconclusive
M2				
M3	Decreased roughness		No significant change	No significant change
<i>Increasing exposure from <math>8.4</math> to <math>25.2 \times 10^5</math> ppm·h</i>				
M1	Inconclusive	Reduction in additives	Increase in contact angle	Decrease in resistance
M2	Increased porosity	Reduction in additives and disruption of PVDF skeleton	No significant change	
M3	Increased roughness			
M3	Decreased roughness		Increase in contact angle with highest exposure	No significant change

hydrophilicity was expected for the membranes with increased chemical exposure, the membranes were still expected to remain hydrophilic.

3.2.3. Contact angle

The impact of varying NaOCl exposure on the relative hydrophilicity of M1, M2, and M3 was estimated by contact angle measurements (Fig. 4). Contact angles for all the membranes increased with NaOCl

exposure to between 25 and 55° confirming our observations in the FTIR analysis above and indicating the membranes remained hydrophilic. M1 and M3 were found to display mild fluctuations ( $\pm 10^\circ$ ) till  $8.4 \times 10^5$  ppm·h and  $16.8 \times 10^5$  ppm·h, respectively, after which the contact angle was observed to increase, hence implying a reduction in hydrophilicity with extended chemical exposure, while the contact angle of M2 was found to remain relatively constant with exposure (Table 5). A reduction in hydrophilicity with chemical exposure, as observed for M1 and M3, was an expected result of the loss in additives observed with FTIR analysis (Fig. 3). Reductions in hydrophilicity of PVDF membranes due to the loss of additives with NaOCl exposure has also been widely reported previously [2,40,47]. The relatively constant contact angle of M2 could have a few explanations. Firstly, the dislodgement of additives did not induce a significant change in surface hydrophilicity for the M2 membrane since the additives remained after chemical exposure, as discussed in Section 3.2.2. Secondly, the increased surface roughness, porosity and potentially increased pore size of the M2 membrane (Fig. 2) may have reduced the effective contact angle due to disruption of the water-membrane interface with additional roughness and porosity, and the capillary effect of pores [5,45]. Finally, it is also possible that the hydrophilicity of M2 may have increased with exposure due to the generation of carbonyl groups resulting from the dehydrofluorination degradation process, as has been reported previously [53,38]. While a reduction in the fluorocarbon group absorbance was observed (1000–1100 cm<sup>-1</sup>), as identified in Section 3.2.2, the typical generation of carbon-carbon double bonds observed at 1590 cm<sup>-1</sup> with dehydrofluorination [13,16] was not found in the FTIR results of this study (see Figure S3 for M2 FTIR spectra). Thus, further investigation would be required to affirm the dehydrofluorination theory.

It should be noted that large fluctuations in initial contact angle, that has been observed in previous studies applying accelerated bench-scale

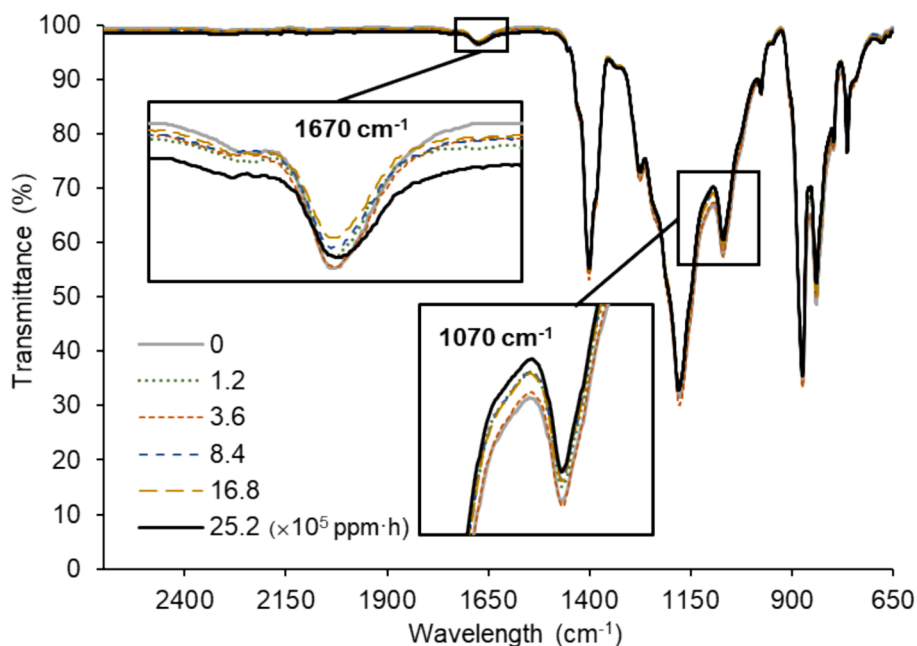


**Fig. 3.** FTIR spectra for M3 membrane with varying NaOCl exposure time. Regions of interest including carbonyl groups at  $1670\text{ cm}^{-1}$  and fluorocarbons at  $1070\text{ cm}^{-1}$  were magnified. FTIR spectral changes for M1 and M2 over the range of exposures can be found in Section S4.

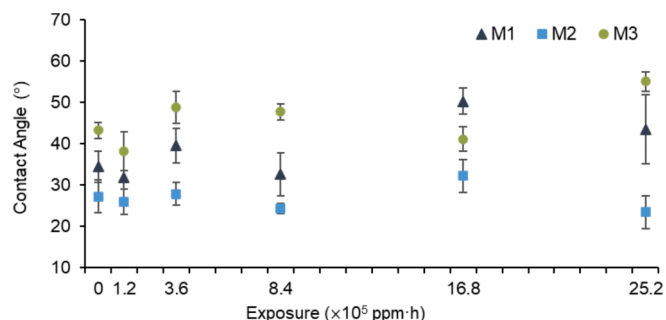


**Fig. 4.** Contact angle for M1, M2 and M3 with varying NaOCl exposure time. See Section 2.1.2 for details on contact angle analysis. Error was calculated as the standard deviation of contact angles across 5 measurements taken for each data point. A one-way ANOVA was conducted on the contact angles to determine the significance of variance in the results, see Section S6 for details.

ageing tests [29,38], was not found here (Fig. 4), with all membranes displaying minor initial fluctuations ( $\pm 10^\circ$ ) as mentioned previously. The fluctuations observed previously with initial exposures were likely due to varying membrane preparation protocols where the initial wetting of the membrane could be expected through the removal of membrane preservative agents [47,15]. This indicated that that membrane preparation and rinsing protocol used in this study, described in Section 2.1.1, was able to minimise initial fluctuations in apparent hydrophilicity due to contaminating wetting agents that would otherwise pose little significance to long-term membrane ageing effects in industrial operation [47].

### 3.2.4. Clean water resistance

The impact of NaOCl exposure on clean water (deionised water) resistance across the three membranes was found to be in the order  $M1 > M2 > M3$  (Fig. 5). All membranes displayed initial fluctuations in resistance, however, M1 and M2 displayed an overall decline in resistance with extended exposure (Table 5). For M1, the resistance was found to fluctuate by 20 % till  $8.4 \times 10^5\text{ ppm}\cdot\text{h}$ , after which, it decreased between  $-15\%$  to  $-25\%$  of the original resistance. In the case of M2,

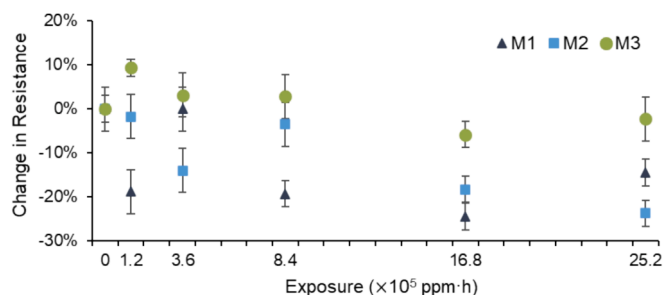


**Fig. 5.** Change in clean water resistance for M1, M2, and M3 with varying NaOCl exposure time at pH 10.5. Error in clean water resistance was calculated from the standard deviation of resistance measurement taken every 30 s over 3 mins. See Section 2.2.2 for details on clean water resistance measurement.

membrane resistance fluctuated by 10–15 % till  $16.8 \times 10^5\text{ ppm}\cdot\text{h}$  after which it declined by 25 % at the highest exposure. The fluctuating initial clean water resistances of M1 and M2 below the original resistance could indicate an unstable initial pore size as additives gradually degraded and/or removed from the PVDF framework [53,40]. Resistance fluctuations could also be a result of the changing hydrophilicity of the membranes as the two parameters are interdependent [45,29], however, the effects of pore size on resistance has been reported to dominate over hydrophilicity [53]. Moreover, the final decrease in resistance observed here was also found in previous studies that reported resistance decline due to pore enlargement resulting from the loss of additives and potential PVDF chain scission [15,29]. It is important to note that the high impact of chemical exposure on the clean water resistance of M1 indicated that the physical degradation and potential increase in pore size previously noted for M2 also occurred in M1. This was despite inconclusive evidence obtained from SEM and FTIR analysis for the M1 membrane. Unlike M1 and M2, M3 displayed a relatively stable clean water resistance, where the measured resistance till the maximum  $25.2 \times 10^5\text{ ppm}\cdot\text{h}$  exposure did not change by over 10 %. This may have been due to the low initial resistance of the M3 membrane due to larger original pore size (Table 1), thus resulting in less significant impact of additive loss inducing pore enlargement on the resistance decline of M3



compared to M1 and M2.

### 3.3. Impact of hypochlorite ageing on fouling behaviour

#### 3.3.1. Fouling rate

The fouling rate for the filtration of M1, M2, and M3 with algal protein feed was observed with increasing NaOCl exposure time (Fig. 6). The relative performance of the membranes throughout tested chemical exposures corresponded with the general conclusions drawn in Section 3.1 (Table 4). A higher overall fouling rate was found for M1, likely indicating that M1 presented smaller pores compared to M2 and M3 throughout tested exposures that thus led to increased overall filtration resistance [7,27]. Moreover, the correlation of M1 with the cake filtration model ( $R^2 > 0.99$ ) (Table 3) in Cycle 1 indicated that the membrane may have rapidly surpassed the initial interaction between foulants and membrane. The higher overall fouling rate of M1 across the initial cycles could reflect the resistance rate of the fouling layer itself and the interaction between foulants during filtration [54]. Exponential development of fouling over 6 cycles was also consistent throughout exposure for M3, likely due to additional pore blocking in larger pores for this membrane, as discussed in Section 3.1.2. The exponential fouling

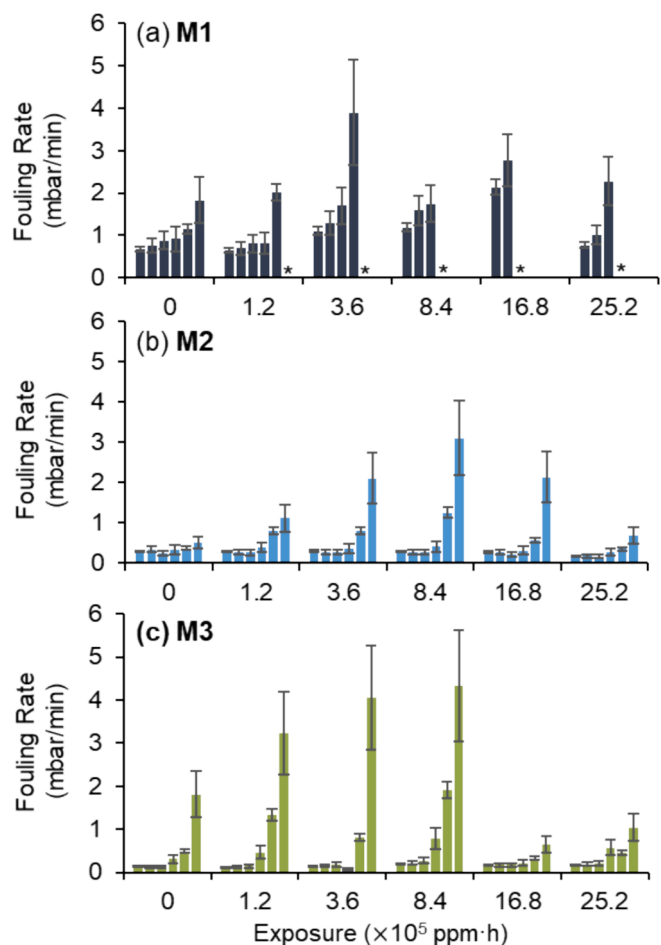
progression for M2 with chemical exposure affirmed the previous findings in Section 3.1.2 that indicated M2 could display similar exponential fouling behaviour to M3 due to higher correlations with pore blocking filtration models with increased cycles (Table 3). Thus, in this study, the relative fouling performance across different membranes in terms of fouling rate and fouling mechanisms was not found to change with chemical exposure time.

Furthermore, for all three membranes, a distinct increase in fouling rate was observed with increasing NaOCl exposure until  $8.4 \times 10^5$  ppm·h for M2 and M3, and  $16.8 \times 10^5$  ppm·h for M1. After these exposures, the fouling rate declined. From the results of membrane characterisation (Table 5), the initial increase in membrane fouling behaviour may have been attributed to decreased membrane hydrophilicity resulting from a reduction in hydrophilic additives from the PVDF framework (Fig. 3), and increased hydrophobic interactions between foulants and the membrane surface. The increasing fouling behaviour due to increased hydrophobicity with NaOCl exposure has also been reported previously [46,40]. Furthermore, the removal of additives from the surface was also likely to induce pore enlargement, as discussed in Section 3.2.4, which has also been reported to aggravate fouling behaviour due to tendency for greater pore blocking [53]. The subsequent decline in fouling rate with high exposure was likely a result of excess pore enlargement, evidenced by the decline in clean water resistance (Fig. 5) that may have reduced membrane selectivity and thus reduced the severity of cake layer formations [40]. Therefore, the fouling rate for all membranes initially increased due to potential reduction in hydrophilicity and increased pore size, and then decreased likely due to excess pore enlargement that could reduce membrane selectivity.

#### 3.3.2. Membrane dissolved organic rejection

The quality of the permeate with increasing NaOCl exposure was presented as the rejection of organic size fractions by the membranes (Fig. 7). For all three membranes, the rejection of biopolymers was above 80 % without NaOCl exposure, thus suggesting that the membrane integrity can be expected to remain intact without chemical ageing over multiple filtration cycles for short-term experiments. The rejection was found to decrease with elevated exposures, thus indicating decreased membrane selectivity with chemical exposure. M1 presented > 90 % biopolymer rejection till  $1.2 \times 10^5$  ppm·h, after which, rejection declined to 65 % at  $25.2 \times 10^5$  ppm·h exposure. However, when considering the error in measurement of biopolymers, M2 and M3 displayed a more notable reduction in biopolymer rejection. M2 and M3 presented a stable biopolymer rejection up to the  $16.8 \times 10^5$  ppm·h exposure, after which the biopolymer rejection dropped significantly to 40 % and 25 % at  $25.2 \times 10^5$  ppm·h for M2 and M3, respectively. The results corresponded with the previously hypothesized decrease in membrane selectivity that likely led to a decline in fouling rate for high exposures (Fig. 6). Thus, all membranes were found to exhibit pore enlargement with chemical exposure that could gradually reduce membrane selectivity [40]. However, it is interesting to note that the M1 membrane presented a more stable rejection of biopolymers through the tested exposures, and the decline in fouling resistance was also found at a later exposure compared to M2 and M3 (Fig. 6). This could potentially be explained by the smaller original pore size of the M1 membrane that could thus endure greater chemical attack before integrity loss. Hence, the smaller pore size of the M1 membrane could have provided a higher chemical resistance to physical degradation leading to loss in membrane selectivity compared to M2 and M3.

For all membranes, the rejection of IMWC and LMWN compounds (Fig. 7), implying the reduction of these compounds in the permeate, could be attributed to removal mostly by adsorption and by retention on secondary cake layer formations. The removal of IMWC was likely primarily governed by adsorption, where rougher membrane surfaces could provide greater surface area for foulant adsorption [23,28]. The rejection of IMWC across the membranes was thus highest for M2 that



\* Data not measured, maximum TMP of 40 kPa reached

**Fig. 6.** Fouling rate for (a) M1, (b) M2, and (c) M3 with varying NaOCl exposure time. Each bar represents the fouling rate of 1 cycle characterised by 2 h filtration followed by 2 min backwash. Filtration was conducted for 6 cycles or until 40 kPa was reached, with an overnight relaxation after the 3rd cycle. For M1, reduced cycles could be performed under 40 kPa due to a higher fouling rate. TMP profiles for each membrane filtration experiment can be found in Section S5. Error in fouling rate was calculated using triplicate fouling experiments conducted with the unaged M3 membrane.



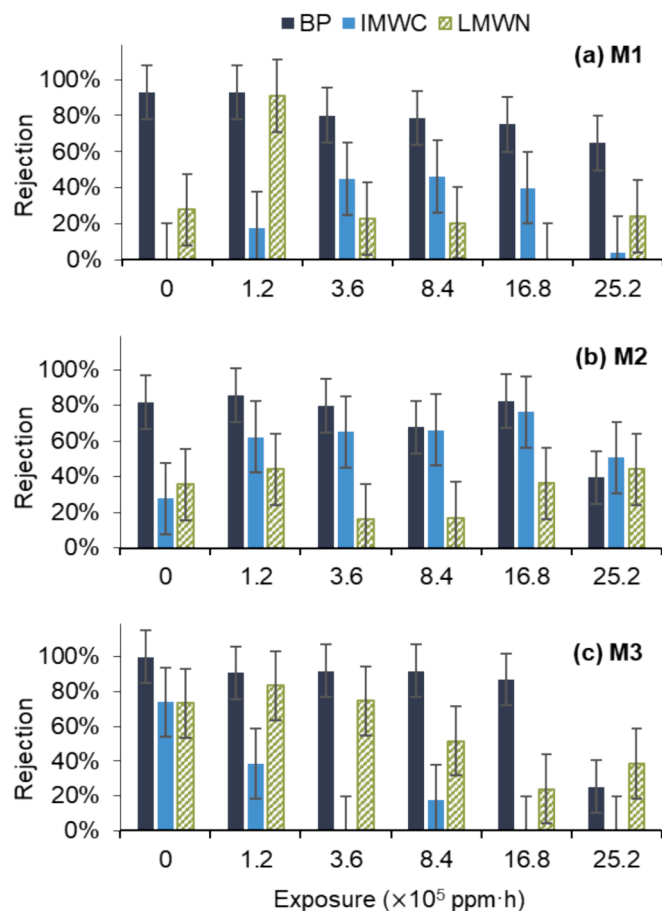


Fig. 7. Organic rejection for membranes (a) M1, (b) M2, and (c) M3 with varying NaOCl exposure. Organic material characterised using LC-OCD analysis, where chromatographed DOC was fractionated into biopolymers (BP), intermediate molecular weight compounds (IMWC), and low molecular weight neutrals (LMWN). Error in organic rejection was calculated using triplicate fouling experiments conducted with the unaged M3 membrane.

presented the greatest overall surface roughness and low for M1 that presented the lowest roughness for all exposures (Fig. 2). Moreover, while IMWC rejection by M3 was high for no exposure, the rejection declined, thus again corresponding with the decreasing roughness previously noted for M3 with increasing NaOCl exposure (Fig. 2). Rejection of LMWN was found to display a distinct decline for higher exposures with M3, where rejection declined after  $1.2 \times 10^5$  ppm·h from ~80 % to 25 % at  $16.8 \times 10^5$  ppm·h. Considering the corresponding decline in membrane fouling rate for M3 (Fig. 6), this likely indicated that the removal of LMWN could be dependent on the development of cake layers on that membrane surface that provide additional opportunity for adsorption [4]. This mechanism of adsorption was likely compounded as the cake layer developed over consecutive filtration cycles. However, trends in the removal of LMWN was not distinct for M1 and M2, likely due to the complex interdependent factors governing LMWN removal by both adsorption on the membrane surface and pores, and secondary cake layer formation.

### 3.3.3. Backwash efficiency

Backwash efficiency for the three membranes at each exposure was determined using the average reversibility after backwash following a filtration cycle (Fig. 8). Initially, increasing chemical exposure led to a decline in the backwash efficiency for M1 from ~55 % to 30 %, while for M2 and M3 the trends fluctuated (~30 to 55 %). However, with the highest exposures, the backwash efficiency for all membranes increased to ~60 %. The initial decline in backwash reversibility for M1

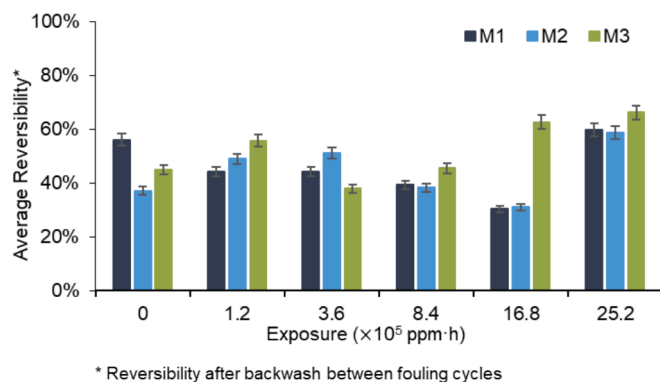


Fig. 8. Average reversibility after backwash for M1, M2 and M3 membranes with varying NaOCl exposure.

corresponded with the potential reduction in hydrophilicity and pore enlargement, discussed in Sections 3.3.1, that also contributed to the corresponding increase in fouling rate (Fig. 6) and decrease in rejection (Fig. 7). The fluctuating trends for M2 and M3 in the initial exposures was likely because the backwash efficiency was sensitive to a range of factors including the changing pore size, surface roughness and degree of fouling deposit. The higher reversibility with the highest exposure for all membranes could be attributed to lower overall fouling deposit implied by the lower fouling rate (Fig. 6) and lower rejection (Fig. 7), as discussed in Sections 3.3.1. Thus, the backwash efficiency for all membranes was likely a result of changing pore size, roughness, and fouling deposit that also impacted the membrane fouling rate and reversibility.

### 3.3.4. Chemically irreversible fouling resistance

Chemically irreversible fouling was assessed using the CIFR for each membrane with increasing NaOCl exposure (Fig. 9). While M1 displayed fluctuating CIFR trends, the CIFR for M3, and M2 to some extent, could be found to correspond with the fouling rate for the membrane. No clear trend was observed for M1 CIFR, potentially due to the varying number of filtration cycles performed for this membrane (Fig. 6) that may have altered the degree of foulant adhesion to the membrane surface or pore walls. The CIFR for M3 displayed an increasing trend till  $8.4 \times 10^5$  ppm·h and then a decrease (Fig. 9), thus corresponding with the respective increase and decrease in fouling rate (Fig. 6). This suggested that the irreversible fouling deposit in M3 was aggravated with higher overall fouling deposit. This was likely due to more severe fouling via pore blocking in M3, as discussed in Section 3.3.1, that increased chemically irreversible deposit. A similar trend in CIFR was observed for M2 between  $1.2 \times 10^5$  ppm·h and  $16.8 \times 10^5$  ppm·h (Fig. 9), though with a lower magnitude in resistance that may have been sensitive to experimental variations. Thus, while the results were largely inconclusive for M1 and M2, the irreversible fouling for M3 was found to

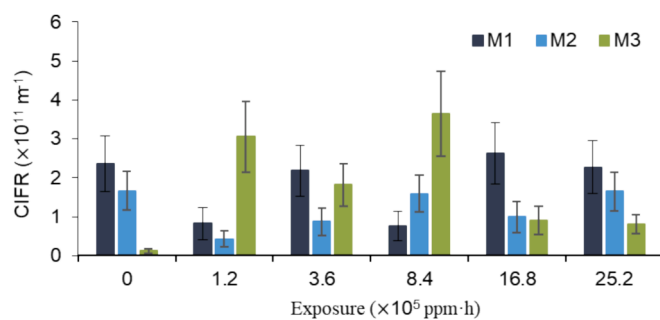


Fig. 9. Chemically irreversible fouling resistance (CIFR) for M1, M2, and M3 membranes with varying NaOCl exposure. Error was calculated as the sum of the standard deviation of resistance measurements before and after fouling.

correspond with the degree of fouling deposit on the membrane due to more severe pore blocking in membranes with larger pores.

It was noted that the CIFR was below 15 % of the fouling resistance accrued over the fouling cycles for all membranes across the NaOCl exposures tested (refer to TMP profiles in Section S5). Thus, all membranes presented relatively low CIFR despite chemical ageing. This could be attributed to high chemical resistance of the membranes, the nature of the feed solution, and the cleaning regime applied. The aggregation of the algal protein feed solution, as described in Section 2.2.1, resulted in a large proportion of fouling resistance consisting of loose cake layer deposits that were readily detached from the membrane during the backwash and chemical cleaning regime. Furthermore, it is important to note that only a single point resistance measurement at  $100 \text{ L}\cdot\text{m}^{-2}\cdot\text{h}^{-1}$  was applied in this study. Multiple point resistance measurements at stepped flux intervals could be used in future work to obtain a more robust resistance measurement, and potentially to better understand the nature of the irreversible fouling layers on each membrane.

#### 4. Conclusions

The impact of membrane characteristics and chemical ageing in 5000 ppm NaOCl at pH 10.5 on fouling behaviour by algal protein was explored in this study. Distinct fouling mechanisms and reversibility trends were found for the three PVDF UF membranes due to differences in pore size and surface roughness. The membrane with smaller pore size and smoother surface (M1) presented higher physical reversibility and more stable fouling performance compared to membranes featuring rougher surfaces (M2) or larger pores (M3). This was attributed to greater foulant attachment on rough membrane surfaces that reduced physical reversibility and more pore blocking with larger pore size that resulted in increasing fouling rate. The observed differences in membrane performance across the membranes highlighted the potential for fine-tuning PVDF membrane characteristics to obtain desired advantages such as low filtration resistance or higher cleaning efficiency. In this study, typical pore blocking and cake filtration models were used to provide an insight into the types of preferential fouling mechanisms during filtration. However, it was noted that fouling likely involved a combination of fouling mechanisms. It is therefore recommended that future work apply the use of combined fouling models to better elucidate the type of fouling mechanisms throughout filtration. Moreover, it was also noted that factors other than surface filtration may also dictate the fouling behaviour observed across the membranes, particularly in the case of M2. Further study is required to better understand the impact of depth filtration effects caused by the internal structure and morphology of the membrane selective and support layers on the fouling and rejection of the membranes.

With chemical ageing, the membrane with the smallest original pore size (M1) was found to present the highest potential resistance to chemical degradation and maintained high membrane selectivity for high exposures. Thus, the study demonstrated that membrane modifications to induce smaller pore size could increase the longevity of membrane filtration performance with high chemical exposure in feedwaters containing algal protein. It is recommended to further investigate changes in membrane properties and fouling behaviour with more NaOCl exposure intervals between  $8.4 \times 10^5 \text{ ppm}\cdot\text{h}$  and  $25.2 \times 10^5 \text{ ppm}\cdot\text{h}$ , where significant changes were observed in fouling rate, rejection, and backwash efficiency. More robust and quantitative methods of measuring surface roughness, porosity and pore size of the membranes could provide greater detail into the fouling performance observed for each membrane with increasing chemical exposure. For example, more detailed characterisation of changes in surface roughness and pore size distribution with chemical exposure could lend insights into the different LMWN rejection and irreversible fouling resistances observed after ageing. Extended characterisation by atomic force microscopy (AFM) could be used to provide a more quantitative assessment

of surface roughness and is thus recommended to be conducted in addition to SEM analysis in future studies on membrane ageing. The purpose of the methods used in the present study was to provide a qualitative differentiation between the three membranes and identify prominent membrane characteristics contributing to fouling and ageing performance. It should be noted that assessing the individual impact of each physical membrane parameter can be challenging due to the interrelated nature of membrane surface, selective layer and support layer characteristics and morphology. Therefore, methods such as principal component analysis is recommended for future studies applying quantitative methods for membrane characterisation towards understanding their impact on membrane fouling behaviour.

#### CRediT authorship contribution statement

**Zainab Z. Mustafa:** Writing – review & editing, Writing – original draft, Formal analysis, Data curation, Conceptualization. **Adrian T. Murdock:** Writing – review & editing, Conceptualization. **Zongli Xie:** Writing – review & editing, Supervision, Conceptualization. **Geoffrey Johnston-Hall:** Writing – review & editing, Supervision, Resources, Project administration, Methodology, Funding acquisition, Conceptualization. **Rita K. Henderson:** Writing – review & editing, Supervision, Methodology. **Greg L. Leslie:** Writing – review & editing, Supervision, Conceptualization. **Pierre Le-Clech:** Writing – review & editing, Supervision, Resources, Project administration, Methodology, Funding acquisition, Conceptualization.

#### Declaration of competing interest

The authors declare that they have no known competing financial interests or personal relationships that could have appeared to influence the work reported in this paper.

#### Data availability

The data that has been used is confidential.

#### Acknowledgements

This research was sponsored by DuPont Water Technologies as part of the UNSW-CSIRO Industry PhD Program and an Australian Commonwealth Research Training Program (RTP) scholarship. The authors would like to thank Bruce Biloft and Christopher Kersten for their support during the development of this research.

#### Appendix A. Supplementary data

Supplementary data to this article can be found online at <https://doi.org/10.1016/j.seppur.2024.128481>.

#### References

- [1] A. Abdelrasoul, H. Doan, A. Lohi, A mechanistic model for ultrafiltration membrane fouling by latex, *J. Membr. Sci.* 433 (2013) 88–99.
- [2] S.Z. Abdullah, P.R. Bérubé, Assessing the effects of sodium hypochlorite exposure on the characteristics of PVDF based membranes, *Water Res.* 47 (2013) 5392–5399.
- [3] S.Z. Abdullah, P.R. Bérubé, Filtration and cleaning performances of PVDF membranes aged with exposure to sodium hypochlorite, *Sep. Purif. Technol.* 195 (2018) 253–259.
- [4] S.A. Alizadeh tabatabai, J.C. Schippers, M.D. Kennedy, Effect of coagulation on fouling potential and removal of algal organic matter in ultrafiltration pretreatment to seawater reverse osmosis, *Water Res* 59 (2014) 283–294.
- [5] E. Arkhangelsky, D. Kuzmenko, V. Gitis, Impact of chemical cleaning on properties and functioning of polyethersulfone membranes, *J. Membr. Sci.* 305 (2007) 176–184.
- [6] S. Ashtiani, M. Khoshnamvand, P. Číhal, M. Dendisová, A. Randová, D. Bouša, A. Shalutina-Kolešová, Z. Sofer, K. Friess, Fabrication of a PVDF membrane with tailored morphology and properties via exploring and computing its ternary phase

- diagram for wastewater treatment and gas separation applications, *RSC Adv.* 10 (2020) 40373–40383.
- [7] M.R. Bilal, H.A. Arfat, I.F.J. Vankelecom, Membrane technology in microalgae cultivation and harvesting: a review, *Biotechnol. Adv.* 32 (2014) 1283–1300.
  - [8] B. Blankert, B. van der Bruggen, A.E. Childress, N. Ghaffour, J.S. Vrouwenvelder, Potential pitfalls in membrane fouling evaluation merits of data representation as resistance instead of flux decline in membrane filtration, *Membranes* 11 (2021) 460.
  - [9] H. Chang, F. Qu, H. Liang, R. Jia, H. Yu, S. Shao, K. Li, W. Gao, G. Li, Correlating ultrafiltration membrane fouling with membrane properties, water quality, and permeate flux, *Desalin. Water Treat.* 56 (2015) 1746–1757.
  - [10] N.G. Cogan, D. Ozturk, K. Ishida, J. Safarik, S. Chellam, Membrane aging effects on water recovery during full-scale potable reuse: mathematical optimization of backwashing frequency for constant-flux microfiltration, *Sep. Purif. Technol.* 286 (2022) 120294.
  - [11] J. Delattre, B. Rabaud, A. Bréhan, K. Glucina, C. Sollogoub, F. Thomine, Ageing of hollow fiber membranes in polyvinylidene fluoride (pvdf) used in water treatment, *Procedia Eng.* 44 (2012) 764–767.
  - [12] F. Gao, J. Wang, H. Zhang, H. Jia, Z. Cui, G. Yang, Aged PVDF and PSF ultrafiltration membranes restored by functional polydopamine for adjustable pore sizes and fouling control, *J. Membr. Sci.* 570–571 (2019) 156–167.
  - [13] F. Gao, J. Wang, H. Zhang, Y. Zhang, M.A. Hang, Effects of sodium hypochlorite on structural/surface characteristics, filtration performance and fouling behaviors of PVDF membranes, *J. Membr. Sci.* 519 (2016) 22–31.
  - [14] M. Gryta, J. Grzechulska-Damszel, A. Markowska-Szczupak, K. Karakulski, The influence of polypropylene degradation on the membrane wettability during membrane distillation, *J. Membr. Sci.* 326 (2009) 493–502.
  - [15] S. Hajibabania, A. Antony, G. Leslie, P. Le-Clech, Relative impact of fouling and cleaning on PVDF membrane hydraulic performances, *Sep. Purif. Technol.* 90 (2012) 204–212.
  - [16] N.A. Hashim, Y. Liu, K. Li, Stability of PVDF hollow fibre membranes in sodium hydroxide aqueous solution, *Chem. Eng. Sci.* 66 (2011) 1565–1575.
  - [17] M. Hashino, T. Katagiri, N. Kubota, Y. Ohmukai, T. Maruyama, H. Matsuyama, Effect of surface roughness of hollow fiber membranes with gear-shaped structure on membrane fouling by sodium alginate, *J. Membr. Sci.* 366 (2011) 389–397.
  - [18] J. Hong, Y. He, Effects of nano sized zinc oxide on the performance of PVDF microfiltration membranes, *Desalination* 302 (2012) 71–79.
  - [19] L. Hou, Z. Wang, P. Song, A precise combined complete blocking and cake filtration model for describing the flux variation in membrane filtration process with BSA solution, *J. Membr. Sci.* 542 (2017) 186–194.
  - [20] B. Huang, H. Gu, K. Xiao, F. Qu, H. Yu, C. Wei, Fouling mechanisms analysis via combined fouling models for surface water ultrafiltration process, *Membranes* 10 (2020) 149.
  - [21] W. Huang, Y. Zhu, B. Dong, W. Lv, Q. Yuan, W. Zhou, W. Lv, Investigation of membrane fouling mechanism of intracellular organic matter during ultrafiltration, *Sci. Rep.* 11 (2021) 1012.
  - [22] K.-J. Hwang, C.-Y. Liao, K.-L. Tung, Effect of membrane pore size on the particle fouling in membrane filtration, *Desalination* 234 (2008) 16–23.
  - [23] O.T. Iorhemen, R.A. Hamza, J.H. Tay, Membrane bioreactor (MBR) technology for wastewater treatment and reclamation membrane fouling, *Membranes* 6 (2016) 33.
  - [24] E. Iritani, N. Katagiri, Developments of blocking filtration model in membrane filtration, *Kona Powder Part. J.* 2016 (2016) 179–202.
  - [25] E. Iritani, N. Katagiri, T. Takenaka, Y. Yamashita, Membrane pore blocking during cake formation in constant pressure and constant flux dead-end microfiltration of very dilute colloids, *Chem. Eng. Sci.* 122 (2015) 465–473.
  - [26] I.A. Khan, J.-O. Kim, Role of inorganic foulants in the aging and deterioration of low-pressure membranes during the chemical cleaning process in surface water treatment: a review, *Chemosphere* 341 (2023) 140073.
  - [27] P. Krzeminski, L. Leverette, S. Malamis, E. Katsou, Membrane bioreactors – a review on recent developments in energy reduction, fouling control, novel configurations, LCA and market prospects, *J. Membr. Sci.* 527 (2017) 207–227.
  - [28] R. Kumar, A.F. Ismail, Fouling control on microfiltration/ultrafiltration membranes effects of morphology, hydrophilicity, and charge, *J. Appl. Polym. Sci.* 132 (2015).
  - [29] I. Levitsky, A. Duek, E. Arkhangelsky, D. Pinchev, T. Kadoshian, H. Shetrit, R. Naim, V. Gitis, Understanding the oxidative cleaning of UF membranes, *J. Membr. Sci.* 377 (2011) 206–213.
  - [30] K. Li, Q. Su, S. Li, G. Wen, T. Huang, Aging of PVDF and PES ultrafiltration membranes by sodium hypochlorite: effect of solution pH, *J. Environ. Sci.* 104 (2021) 444–455.
  - [31] Y. Liao, A. Bokhary, E. Maleki, B. Liao, A review of membrane fouling and its control in algal-related membrane processes, *Bioresour. Technol.* 264 (2018) 343–358.
  - [32] L. Marbelia, M. Mulier, D. Vandamme, K. Muylaert, A. Szymczyk, I.F. J. Vankelecom, Polyacrylonitrile membranes for microalgae filtration: influence of porosity, surface charge and microalgae species on membrane fouling, *Algal Res.* 19 (2016) 128–137.
  - [33] S. Menon, K. Bansode, S. Nandi, V. Kalyanraman, Impact of cleaning agents on properties of tubular polyvinylidene fluoride (PVDF) membrane, *Mater. Today: Proc.* 47 (2021) 1466–1471.
  - [34] D.J. Miller, D.R. Dreyer, C.W. Bielawski, D.R. Paul, B.D. Freeman, Surface modification of water purification membranes, *Angew. Chem. Int. Ed. Engl.* 56 (2017) 4662–4711.
  - [35] Z.Z. Mustafa, N.R.H. Rao, R.K. Henderson, G.L. Leslie, P. Le-Clech, Considerations of the limitations of commonly applied characterisation methods in understanding protein-driven irreversible fouling, *Environ. Sci. Water Res. Technol.* 8 (2022) 343–357.
  - [36] Z.Z. Mustafa, N.R.H. Rao, G. Johnston-Hall, R.K. Henderson, G.L. Leslie, P. Le-Clech, Membrane fouling during algal blooms: Impact of extracellular algal organic matter feed and membrane surface properties, *J. Environ. Chem. Eng.* 10 (2022) 108749.
  - [37] B. Pellegrin, F. Mezzari, Y. Hanafi, A. Szymczyk, J.-C. Remigy, C. Causserand, Filtration performance and pore size distribution of hypochlorite aged PES/PVP ultrafiltration membranes, *J. Membr. Sci.* 474 (2015) 175–186.
  - [38] V. Puspitasari, A. Granville, P. Le-Clech, V. Chen, Cleaning and ageing effect of sodium hypochlorite on polyvinylidene fluoride (PVDF) membrane, *Sep. Purif. Technol.* 72 (2010) 301–308.
  - [39] M. Rabiller-Baudry, P. Loulergue, J. Girard, M. El mansour el jastimi, A. Bouzin, M. Le gallic, A. Moreac, P. Rabiller, Consequences of membrane aging on real or misleading evaluation of membrane cleaning by flux measurements, *Sep. Purif. Technol.* 259 (2021) 118044.
  - [40] M.F. Rabuni, N.M. Nik Sulaiman, M.K. Aroua, C. Yern chee, N. Awanis Hashim, Impact of in situ physical and chemical cleaning on PVDF membrane properties and performances, *Chem. Eng. Sci.* 122 (2015) 426–435.
  - [41] J. Ravereau, A. Fabre, A. Brehant, R. Bonnard, C. Sollogoub, J. Verdu, Ageing of polyvinylidene fluoride hollow fiber membranes in sodium hypochlorite solutions, *J. Membr. Sci.* 505 (2016) 174–184.
  - [42] C. Regula, E. Carretier, Y. Wyart, G. Gésan-Guizieu, A. Vincent, D. Boudot, P. Moulin, Chemical cleaning/disinfection and ageing of organic UF membranes a review, *Water Res.* 56 (2014) 325–365.
  - [43] A. Resosudarmo, Y. Ye, P. Le-Clech, V. Chen, Analysis of UF membrane fouling mechanisms caused by organic interactions in seawater, *Water Res.* 47 (2013) 911–921.
  - [44] M. Rickman, J. Pellegrino, R. Davis, Fouling phenomena during membrane filtration of microalgae, *J. Membr. Sci.* 423–424 (2012) 33–42.
  - [45] S. Robinson, S.Z. Abdullah, P. Bérubé, P. Le-Clech, Ageing of membranes for water treatment Linking changes to performance, *J. Membr. Sci.* 503 (2016) 177–187.
  - [46] S. Robinson, P.R. Bérubé, Membrane ageing in full-scale water treatment plants, *Water Res.* 169 (2020) 115212.
  - [47] S.J. Robinson, P.R. Bérubé, Seeking realistic membrane ageing at bench-scale, *J. Membr. Sci.* 618 (2021) 118606.
  - [48] P. Sanaei, L.J. Cummings, Flow and fouling in membrane filters: effects of membrane morphology, *J. Fluid Mech.* 818 (2017) 744–771.
  - [49] N. Subhi, A.R.D. Verliefde, V. Chen, P. Le-Clech, Assessment of physicochemical interactions in hollow fibre ultrafiltration membrane by contact angle analysis, *J. Membr. Sci.* 403–404 (2012) 32–40.
  - [50] D.Y. Tan, T. Hashimoto, S. Takizawa, 3D modeling of PVDF membrane aging using scanning electron microscope and OpenCV image analysis, *J. Membr. Sci.* 666 (2023) 121141.
  - [51] K.H. Tng, A. Antony, Y. Wang, G.L. Leslie, 11 - Membrane ageing during water treatment: Mechanisms, monitoring, and control, in: A. Basile, A. Cassano, N.K. Rastogi (Eds.), *Advances in Membrane Technologies for Water Treatment*. Oxford: Woodhead Publishing, 2015.
  - [52] Z. Wang, J. Ma, Q. Liu, Pure sponge-like membranes bearing both high water permeability and high retention capacity, *Desalination* 278 (2011) 141–149.
  - [53] Q. Wu, X. Zhang, G. Cao, Impacts of sodium hydroxide and sodium hypochlorite aging on polyvinylidene fluoride membranes fabricated with different methods, *J. Environ. Sci.* 67 (2018) 294–308.
  - [54] H. Xu, K. Xiao, X. Wang, S. Liang, C. Wei, X. Wen, X. Huang, Outlining the roles of membrane-foulant and foulant-foulant interactions in organic fouling during microfiltration and ultrafiltration: a mini-review, *Front. Chem.* 8 (2020) 417.
  - [55] H. Xu, K. Xiao, J. Yu, B. Huang, X. Wang, S. Liang, C. Wei, X. Wen, X. Huang, A Simple method to identify the dominant fouling mechanisms during membrane filtration based on piecewise multiple linear regression, *Membranes* 10 (2020) 171.
  - [56] H. Yu, S. Shangguan, H. Yang, H. Rong, F. Qu, Chemical cleaning and membrane aging of poly(vinylidene fluoride) (PVDF) membranes fabricated via non-solvent induced phase separation (NIPS) and thermally induced phase separation (TIPS), *Sep. Purif. Technol.* 313 (2023) 123488.
  - [57] Y. Zhang, J. Wang, F. Gao, Y. Chen, H. Zhang, A comparison study the different impacts of sodium hypochlorite on PVDF and PSF ultrafiltration (UF) membranes, *Water Res.* 109 (2017) 227–236.
  - [58] C. Zhao, J. Xue, F. Ran, S. Sun, Modification of polyethersulfone membranes – a review of methods, *Prog. Mater. Sci.* 58 (2013) 76–150.
  - [59] X. Zheng, D. Dai, H. Hua, D. Yu, R. Cheng, L. Zheng, Aging behavior and mechanism of polyvinylidene fluoride membrane by intensified UV irradiation and NaOCl a comparative study, *Process Saf. Environ. Prot.* 180 (2023) 923–934.